Journal of Alloys and Compounds 868 (2021) 159281

Contents lists available at ScienceDirect

Journal of Alloys and Compounds

journal homepage: www.elsevier.com/locate/jalcom

A high-response ultraviolet photodetector by integrating GaN nanoparticles with graphene

Yang Chen[a,b], You Wu[a,b], Jianwei Ben[a,b], Ke Jiang[a,b], Yuping Jia[a,b], Shanli Zhang[a,b], Hang Zang[a,b], Zhiming Shi[a,b], Bin Duan[c,*], Xiaojuan Sun[a,b,**], Dabing Li[a,b]

[a] State Key Laboratory of Luminescence and Applications, Changchun Institute of Optics, Fine Mechanics and Physics, Chinese Academy of Sciences, Changchun 130033, China
[b] Center of Materials Science and Optoelectronics Engineering, University of Chinese Academy of Sciences, Beijing 100049, China
[c] College of Physics, Jilin University, Changchun 130012, China

ARTICLE INFO

Article history:
Received 17 December 2020
Received in revised form 16 February 2021
Accepted 17 February 2021
Available online 20 February 2021

Keywords:
GaN nanoparticles
Graphene
Ultraviolet photodetectors
Kelvin probe force microscope

ABSTRACT

A new type of ultraviolet photodetector was fabricated by integrating GaN nanoparticles as the absorber and graphene as the carrier transport channel. The GaN nanoparticles prepared by metal-organic chemical vapor deposition exhibited the average diameter, height and density of 87.2 nm, 18.4 nm and 5 × 10^9/cm^2, respectively. The chemical component and optical properties of the GaN nanoparticles were also confirmed and discussed. The monolayer graphene film was transferred onto GaN nanoparticles for the detector fabrication, which possessed the high crystalline quality and uniform coverage. Since the GaN nanoparticles providing trap states for the photo-generated hole, a longer carrier lifetime and higher gain would be obtained. In addition, based on the high carrier mobility of the graphene, the ultraviolet photodetector exhibited a persistent photoconduction effect and achieved a high responsivity of 200.69 A/W. The Kelvin probe force microscope measurements were carried out to reveal the device work mechanism and the carrier transport model has been established according to the decreased graphene surface potential of 0.2 eV before and after contacting with the GaN nanoparticles. Present work provides a method for obtaining new types of III-nitrides-based ultraviolet photodetectors with high response.

1. Introduction

Ultraviolet (UV) photodetectors (PDs) with high response are essential for both civilian and military demands, such as fire monitor, flaw detection, biological imaging, and missile warning [1–4]. Till now, GaN epilayer has been widely used as the UV absorber of PDs due to its wide direct bandgap of 3.4 eV. In addition, the unique properties of high breakdown voltage and chemical/thermal tolerance have made GaN-based UV PDs excellent stability and lifetime [5,6]. Among the various device structures of the UV PDs, the metal-semiconductor-metal (MSM) has exhibited the advantages of a low-cost and easy fabrication process [2,7]. Therefore, the UV PDs with metal-GaN-metal structures have been widely applied. Unfortunately, the lattice and thermal mismatch during GaN heteroepitaxy on foreign substrates have induced high-density dislocations (TDs) and point defects in the epitaxial materials [8]. These defects in GaN epilayer act as the scattering/ recombination centers for photo-generated carriers, which hinder the separation of electron-hole pairs and the extraction of the photo-electric signal by the metal electrodes, and thus restricting the deeper development of GaN materials in high-response UV PDs.

Beyond GaN epilayer, the micro- and nano-structures including columns, wires, hexagonal pyramids, and particles have exhibited better crystalline quality. It is considered that these low-dimensional structures with large surface-to-volume ratios are beneficial for the strain release and TDs suppression [9]. Heterostructure UV PDs based on one-dimensional $Al_xGa_{1-x}N$ and GaN nanowires have achieved high responsivity of 10^2-10^3 A/W via precisely controlling the junction interface, component and doping [10–12]. For instance, the heterostructure of Ga_2O_3/GaN obtained by partial thermal oxidization of the GaN nanowire was proposed for high-response UV detection. The excellent optical properties of the vertical nanowire structure and the internal gain mechanism resulted in a high responsivity exceeding 550 A/W at −5 V [11]. As the comparison, zero-dimensional GaN nanoparticles (NPs) might be a better choice for UV detection according

* Corresponding author.
** Corresponding author at: State Key Laboratory of Luminescence and Applications, Changchun Institute of Optics, Fine Mechanics and Physics, Chinese Academy of Sciences, Changchun 130033, China.
E-mail addresses: duanbin@jlu.edu.cn (B. Duan), sunxj@ciomp.ac.cn (X. Sun).

https://doi.org/10.1016/j.jallcom.2021.159281
0925-8388/

to their advantages including the easy fabrication process and mass production ability. The Stranski-Krastanov (SK) growth mode is conventionally applied for the synthesis of GaN NPs [13,14], but it relies on the stress accumulation induced by the large lattice mismatch between the epitaxial materials and the underneath substrates. Therefore, the size and density of the different epitaxial materials are hardly controlled on present limited substrates. Besides, the Ga droplet epitaxy based on the vapor-liquid-solid mechanism is another choice, which exhibits advantages of easily tailored size and density for GaN NPs since this growth process is not constrained by the lattice mismatch condition [15–17]. Recently, Hu et al. reported the photodetector with the self-assembled InGaN quantum dots as the light absorber, which exhibited a high gain of 10^9 with the 450 nm light illumination [18]. These results demonstrate that the low-dimensional GaN NPs might also be a better choice as the deeper UV absorber for new types of high-response PDs, however, the UV PDs based on the GaN NPs absorber are still not well studied.

Graphene is a two-dimensional material with ideal optical transparency, adjustable Femi level (E_F), and high carrier mobility, which can competently serve as transparent electrodes as well as carrier transport channels for various optoelectronic devices [19,20]. Moreover, the electronic/magnetic properties and the structural stability of graphene can be controlled by the embedded foreign atoms, such as Cr/Mo [21], N [22] and V/Nb [23]. In addition, graphene also shows great potential for photocatalytic decomposition of water [24]. According to the tremendous performance, the GaN epilayer integrated with graphene has been proposed to fabricate UV PDs [25–29]. In this device structure, graphene plays as the transport channel for the carriers generated from the GaN epilayer, which would increase the carrier collection efficiency due to its high mobility. Although the enhanced performance of these devices has been proved, the responsivity still limited by tens of A/W or even less [25–27]. Several recent works have focused on the graphene and GaN materials optimization for improving the performance of the devices. Shen et al. proved a fast-response UV PDs by transferring the MMA-enabled ultraclean graphene onto GaN epilayer, which achieved the short response time of 0.5/1.12 ms [28]. Moreover, Li et al. used the nanoporous GaN instead of the bulk GaN epilayer as the light absorber and thus the high-porosity nanoporous GaN has significantly enhanced the light harvesting efficiency, resulting in the ultrahigh detectivity of 1×10^{17} Jones [29].

In this work, we reported and fabricated a new type of UV PDs by integrating the GaN NPs absorber with the graphene carrier transport channel. The morphology, chemical component, and optical properties of the GaN NPs were firstly investigated and discussed. After that, monolayer graphene was transferred onto the GaN NPs for the fabrication of UV PDs, which possessed the high crystalline quality and uniform coverage. The corresponding responsivity of the UV PDs was almost two orders of magnitude higher than that of based on the GaN epilayer/graphene, reaching up to 200.69 A/W at the bias voltage of 5 V. The carrier transport model and working mechanism of this GaN NPs/graphene-based UV PDs were confirmed by Kelvin probe force microscope (KFPM). The KPFM results proves that the trap states in GaN NPs extended the lifetime of photogenerated carriers transported into graphene, which induced the persistent photoconduction effect and thus the high response.

2. Experimental section

2.1. Growth of the AlN template and GaN NPs

The schematic diagram of the growth process for the GaN NPs was shown in Fig. 1a-e. Trimethylaluminum (TMAl; Nata Co. Ltd, China), trimethylgallium (TMGa; Nata Co. Ltd, China), and NH_3 (Linde Co. Ltd, China) were supplied as sources of Al, Ga, and N, respectively. The purity of all the above used materials was 99.9999%. Initially, the AlN template was grown on a 2-inch sapphire substrate by the "two-step" growth method in the high-temperature metal organic chemical vapor deposition (HT-MOCVD) system, as shown in Fig. 1b. The growth process of the AlN template was shown in Fig. 1f and the related growth details could be found elsewhere [30]. The growth process for the GaN NPs was also summarized, as shown in Fig. 1g. After the AlN template growth, the chamber was cleaned by venting process to eliminate the Al source. With the H_2 atmosphere, TMGa was firstly injected for 12 s with a flux of 10 sccm when the temperature reached up to 600 ℃ to form the Ga droplets on the AlN template, as shown in Fig. 1c. After

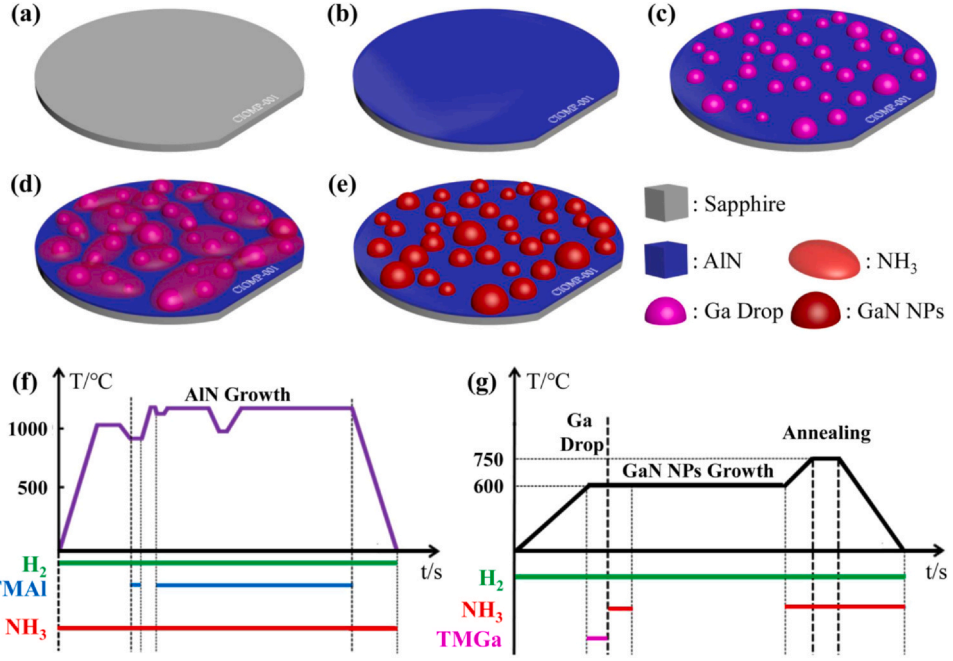

Fig. 1. (a)-(e) Schematic diagram of the growth process for AlN template on sapphire substrates and subsequent GaN NPs on the AlN template by the Ga droplets epitaxy method. (f) Detailed growth steps for AlN template and (g) GaN NPs.

that, a flux of 2000 sccm NH_3 was injected for 12 s and TMGa was simultaneously interrupted. Here, enough time was given for the sufficient reaction of the Ga droplet and NH_3, as shown in Fig. 1d. Finally, the formed GaN NPs was in situ annealed at 750 ℃ for 30 s to improve its crystalline quality, as shown in Fig. 1e.

2.2. Fabrication of UV photodetectors

Monolayer graphene was grown on catalytic Copper foils by the low-pressure chemical vapor deposition (LP-CVD) method, and the graphene was subsequently transferred onto the GaN NPs by a wet transfer strategy. The detailed process could be found in our previous work [31]. The GaN NPs absorber was fully covered by the transferred graphene film, which severed as the transport channel for photo-generated carriers. A pair of patterned Au electrodes with a thickness of 30 nm was deposited on the top of graphene by electron beam evaporation, which severed as the carrier collection pad and also defined the photo-sensitive area of the UV PDs by its length and distance. Here, the photo-sensitive area of the UV PDs was designed as $300 \times 300\ \mu m^2$. As the comparison, the UV PDs were also fabricated on the GaN epilayer with the same device structure. There was no post-annealing process applied to the Au electrodes, which ensured the pristine quality of as-transferred graphene film.

2.3. Characterization and measurement

The morphology of the GaN NPs was measured by scanning electron microscope (SEM; S4800, Hitachi) and atomic force microscope (AFM; MultiMode 8, Bruker). The x-ray photoelectron spectroscopy (XPS; VG ESCALAB MKII, Thermo Scientific) and energy dispersive spectroscopy (EDS; S4800, Hitachi) were applied to obtaining the chemical components of the GaN NPs. The optical properties of the GaN NPs were measured by the temperature-dependent photoluminescence (PL) spectroscopy with a 266 nm laser as the excitation source. Raman spectroscopy (LabRAM HR Evolution, Horiba) with a 532 nm laser was used to evaluating the crystalline quality of the as-transferred graphene on the GaN NPs. Kelvin probe force microscope (KPFM; MultiMode 8, Bruker) was applied to measure the surface potential. The photocurrent and response time of the UV PDs were collected by a 2400 Source Meter (KEITHLEY) and a digital oscilloscope (DS6104, Rigol), respectively. A 266 nm laser (MPL-F-266–20 mW, CNI Laser) with the power density varied from 0.64 to 6.37 mW/mm^2 was severed as the irradiation source.

3. Results and discussion

The cross-sectional image of the as-grown GaN NPs was measured by SEM, as shown in Fig. 2a. The interfaces between the sapphire substrate and AlN template, as well as the AlN template and GaN NPs could be observed. The AlN template owned a thickness of ~1 μm. The GaN NPs with the lateral size lower than 100 nm were randomly distributed on the top of the AlN template. As shown in Fig. S1, the top-view SEM image further proved the random distribution of the GaN NPs and the diameter size was mainly located at the range of 50–115 nm. Due to the limited view field of the GaN NPs in the cross-sectional SEM image, the estimated size had a slight difference compared to that of the top-view SEM image. The two-dimensional and three-dimensional AFM images of the GaN NPs were shown in Fig. 2b and c, both of which the GaN NPs covered on the surface of the underneath AlN template, showing the distribution density of $5 \times 10^9/cm^2$. The statistical parameters of diameter and height of GaN NPs from the three-dimensional AFM images were exhibited in Fig. 2d and e, respectively. The mean diameter of the GaN NPs was calculated to be 87.2 nm with a standard deviation of 15.5 nm and the mean height was 18.4 nm with a standard deviation of 5.4 nm.

The difference in the size of the GaN NPs might be induced during the nitridation of Ga droplets and the later post-annealing of the GaN NPs. As shown in Fig. S2a-b, the enlarged AFM image has exhibited the unsegregated GaN NPs composed of several smaller parts. This phenomenon was consistent with the previously reported works that GaN crystal was primarily formed at the periphery of Ga droplets during NH_3 irradiation and then the high migration of Ga atoms would result in several small GaN crystals in the large Ga droplet [32,33]. The corresponding formation process of the unsegregated GaN NPs was schematically illustrated in Fig. S2d-f. Moreover, one should also consider that the annealing process at a high temperature of 750 ℃ would trigger the decomposition of unstable GaN into Ga and N atoms. Then, the separated Ga atoms with enhanced migration either attached to the periphery of GaN NPs to form larger sizes or evaporated out to reduce the sizes. In this way, the average size and distribution uniformity of the as-grown GaN NPs could be controlled by the parameters of NH_3 flow, reaction pressure, post-annealing temperature, and time in the HT-MOCVD system, which might be presented in our future works.

The chemical components of the GaN NPs were examined by XPS. Fig. 3a showed the full XPS spectra ranged from 0 to 1200 eV and both the Ga 3d and Ga 2p peaks were observed. In order to characterize the chemical bonding of the GaN NPs, the Ga 3d core level in XPS spectra was fitted into four sub-peaks, as shown in Fig. 3b. The corresponding portions were N 2s, Ga metal, Ga–N, and Ga–O, which located at the binding energy of 16.7 eV [34], 18.2 eV [35], 19.9 eV [36], and 20.5 eV [37,38], respectively. The large proportion (88%) of Ga–N bonding in N 2s indicated that the as-grown NPs on the AlN template mainly belonged to the GaN crystal. The Ga metal might be left by the partial reaction of Ga droplets. Therefore, Ga metal would be further oxidized in the atmosphere and forming the Ga–O bonding [32]. As shown in Fig. S3, the EDS spectra of the GaN NPs showed the N and Ga element-related peaks, which further confirmed the formation of GaN crystals in the NPs.

The temperature-dependent (20–300 K) PL spectra of the GaN NPs were shown in Fig. 3c. As the temperature increased from 20 K to 300 K, the PL intensity quenched quickly (disappear at 300 K) due to the temperature-induced non-radiative recombination in the GaN NPs [39]. Since the surface-to-volume ratio of the GaN NPs was larger than that of the GaN epilayer, there were much more surface trap states in GaN NPs, and thus the photo-generated carriers could be quickly driven to its surface trap states at the high temperature of 300 K without any PL emission. However, this process was suppressed at the lower temperature and the radiative recombination was in the domination, leading to the gradually enhanced PL intensity. The PL peak position of the GaN NPs was located at 3.505 eV with the temperature of 20 K, and a total red shift of 58 meV was observed in the range of 20–250 K. It is noted that the large shift of PL position mainly occurred at the temperatures above 80 K (48 meV). As the comparison, the GaN epilayer reported in previous works has exhibited the larger bandgap variation of 67–80 meV [40,41]. Here, different from the GaN epilayer with polar lattice induced by longitudinal optical (LO) phonon coupling, the reduced exciton Bohr radius of the GaN NPs made the less exciton polar and further increased the exciton binding energy [40]. This might demonstrate the reduction of bandgap shift for the GaN NPs with the increased temperature.

As shown in Fig. 4a, the CVD-grown graphene was transferred onto the GaN NPs as the carrier transport channel. The typical SEM image in Fig. 4b exhibited the boundary of the as-transferred graphene (marked by a yellow dash line), and the GaN NPs were uniformly covered by graphene film. No broken area of graphene was observed in the present view field, which indicated that the

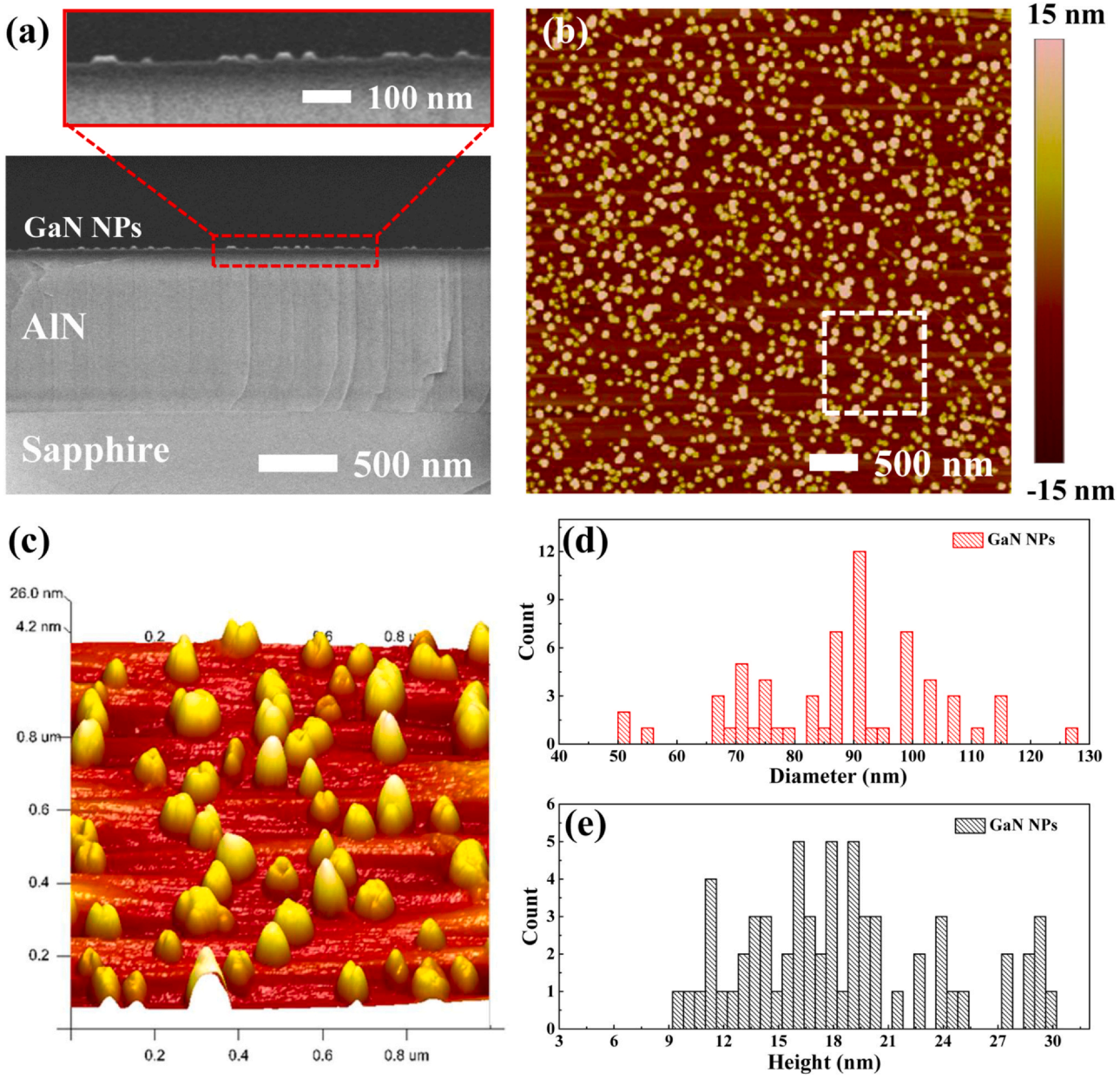

Fig. 2. (a) Cross-sectional SEM image of the GaN NPs on the underneath AlN template/sapphire substrates. (b) The two-dimensional and (c) three-dimensional AFM images of GaN NPs. The three-dimensional image was extracted from the white dash line marked area in (b). (d) Diameter and (e) height distribution for the as-grown GaN NPs.

graphene still maintained its excellent integrity after the transfer process. As shown in Fig. 4c, the SEM image with a larger scan area has exhibited several random wrinkles in the graphene film, which might be caused by the thermal expansion difference between the graphene and underneath substrate [42]. The crystalline quality of graphene on the GaN NPs was further evaluated by Raman spectra, as shown in Fig. 4d. The typical D, G and 2D bands of graphene were observed. The weak intensity of the defect-related D band and the intensity ratio of 2D to G band (> 2) have indicated the high crystalline quality as well as the monolayer nature of this graphene film on the GaN NPs [43,44].

The schematic device structure and optical microscope image of the UV PDs based on the GaN NPs and graphene were shown in Fig. 5a and b, respectively. A pair of symmetric Au electrode was deposited on graphene as the carrier collection pads. The dark current (I_{dark}) of the UV PDs was measured in Fig. S4, which showed that the I_{dark} reached up to 68.5 mA at the bias voltage of 5 V. This was accessible since the Au electrode was deposited on the graphene film with high carrier mobility and electric conductivity. The photocurrent (I_{ph}) of the PDs was defined as the difference between the current at the illuminated (I_{light}) and dark (I_{dark}) conditions:

$$I_{ph} = I_{light} - I_{dark} \quad (1)$$

As shown in Fig. 5c, the photocurrent of UV PDs by integrating the GaN NPs and graphene linearly decreased with the elevated bias voltage from −4–5 V, indicating the excellent ohmic contact between the Au electrode and graphene. Besides, the net photocurrent of UV PDs at the bias voltage of 5 V has elevated with the increase of incident 266 nm laser powers ranged from 0.64 to 6.37 mW/mm^2. The responsivity of the PDs was defined as [45,46]:

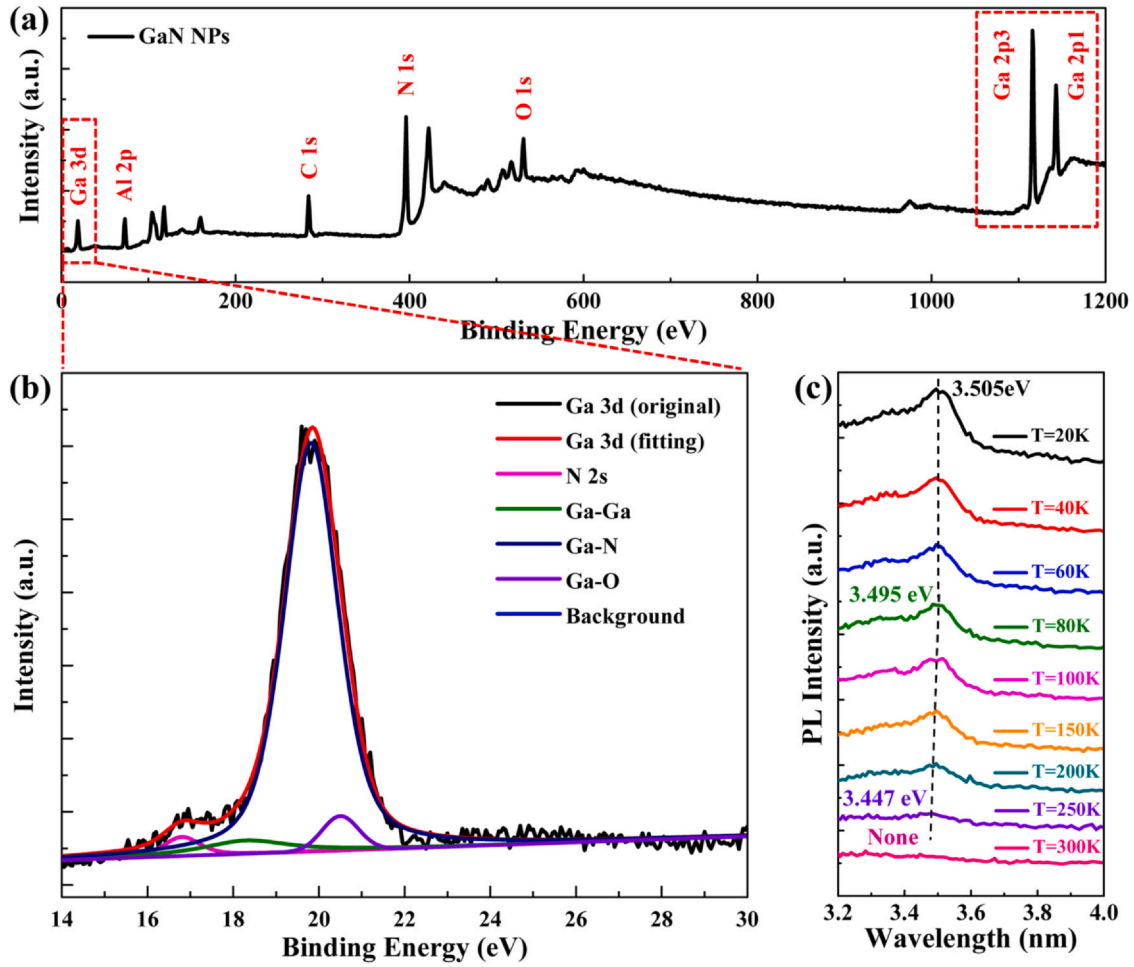

Fig. 3. (a) Full XPS spectra of the GaN NPs. (b) XPS core level spectra of Ga 3d with the fitted sub-peaks of N 2s, Ga–Ga, Ga–N, and Ga–O. (c) Temperature-dependent PL spectra of the GaN NPs ranged from 20 K to 300 K.

$$R = \frac{I_{ph}}{P \times A} \tag{2}$$

where P is the power density of the incident laser and A is the photosensitive area of the PDs. The responsivity of the UV PDs as a function of incident powers was calculated in Fig. 5d, exhibiting that the R decreased with the increase of incident power. The highest responsivity of 200.69 A/W was achieved for the GaN NPs/graphene UV PDs at the bias voltage of 5 V with the incident laser power density of 0.64 mW/mm^2. The photosensitivity (S) and quantum efficiency (η) of the UV PDs could be further estimated from the following equations [47,48]:

$$S = \frac{|I_{ph}|}{I_{dark}} \times 100\% \tag{3}$$

$$\eta = \frac{h \times c}{e \times \lambda} \times R \tag{4}$$

where h is Planck's constant, c is the velocity of light, e is the electron charge, λ is the wavelength of the laser. At the bias voltage of 5 V, the maximum photosensitivity and quantum efficiency of the UV PDs were 52.9% and 0.94×10^3, respectively. According to the response spectra in Fig. 5e, the UV PDs based on GaN NPs and graphene exhibited obvious response when the incident light wavelength below 350 nm, proving the excellent wavelength selectivity in the UV range. The response time of the GaN NPs/graphene UV PDs was shown in Fig. 5f, showing that the rise time and fall time was 186 and 122 ms. Here, the rising range of the signal intensity was related to the light off state. The longer rise time was mainly attributed to the longer carrier lifetime induced by the trap states in the GaN NPs, which have made the photo-generated carriers circuiting in the graphene channel for a longer time even after the light off.

As shown in Fig. S5, the UV PDs with a similar structure was also fabricated on GaN epilayer for comparison, which showed the responsivity and response time of 2.35 A/W and 16.6/7.6 ms, respectively. Compared with the UV PDs based on the conventional GaN epilayer and graphene, the devices with the GaN NPs absorber have the responsivity about two orders of magnitude as well as a relatively longer response time. This has proved that a stronger photoconduction effect might exist in the GaN NPs and graphene system, which was induced by the trap states at the low-dimensional GaN NPs or the interface of GaN NPs/graphene. In this assumption, the photo-generated carriers would be trapped in the GaN NPs, and thus extending their lifetime. Then, the opposite photo-generated carriers drifted into graphene could circulate through the external circuit by the bias voltage for many times, inducing the high responsivity [49]. The performance of the GaN NPs/graphene UV PDs was also compared with previously reported works in Table 1, indicating that the device in this work has exhibited excellent properties, particularly for the responsivity [11,18,25,26,50–53].

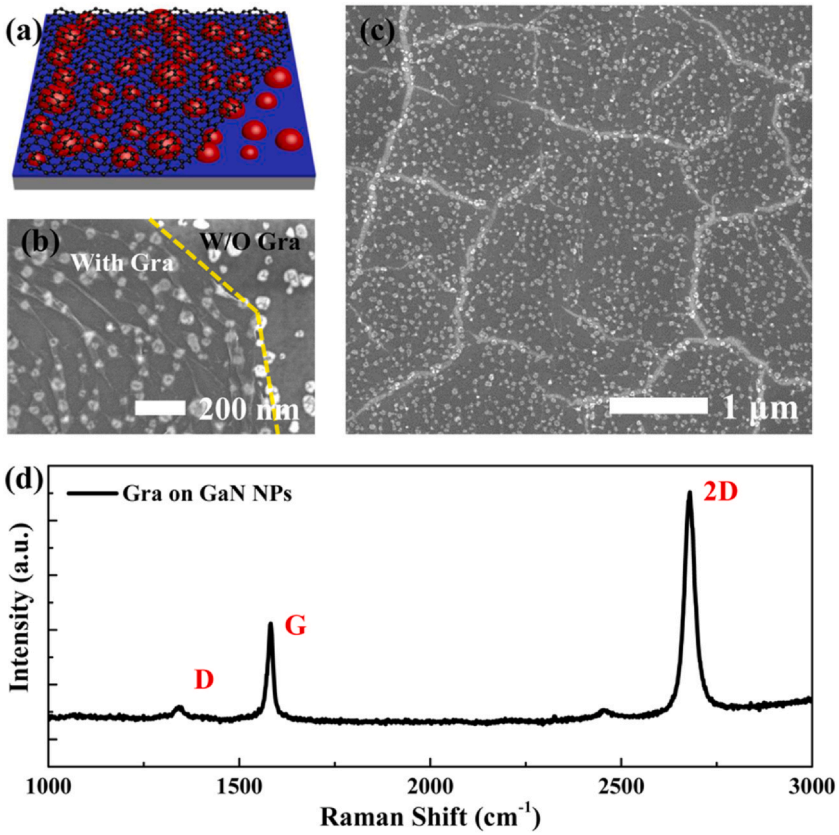

Fig. 4. (a) Schematic diagram of the transferred CVD-grown graphene on the GaN NPs. (b) Typical SEM image and (c) the larger scan area for the graphene covered GaN NPs. (d) Raman spectra of the graphene film transferred onto the GaN NPs. (For interpretation of the references to color in this figure legend, the reader is referred to the web version of this article.)

Beyond the higher gain and longer response time of the GaN NPs/graphene UV PDs, the negative photocurrent and decreased responsivity as the function of the incident powers has been observed in Fig. 5c and d, respectively. In order to figure out the working mechanism of these UV PDs, KPFM was primarily applied to measure the surface potential of separated graphene and graphene contacted with the GaN NPs, which aimed to identify the interfacial potential difference between the GaN NPs and graphene [54], as shown in Fig. 6a and b. Here, a thin layer of Au film was deposited on graphene as the reference base of the surface potential. Assuming that the work function (W_F) of Au is 5.1 eV, the corresponding W_F for separated graphene and graphene contacted with GaN NPs could be calculated to 5.01 and 5.21 eV according to the surface potential difference [55,56]. In this situation, the W_F of the separated graphene was below the Dirac point with p-type dopant due to the polymer residue or oxygen/water absorption on graphene. Once the graphene contacted with the GaN NPs, holes in the GaN NPs were extracted and drifted into graphene due to the strong interfacial polarization effect induced by the energy level mismatch between the GaN NPs and graphene. In this way, the E_F of graphene contacted with GaN NPs has down-shifted 0.2 eV because of its increased hole density compared to the separated graphene. According to the holes transfer, a built-in electric field was simultaneously formed at the interface of graphene and GaN NPs, which pointed from the graphene to GaN NPs.

Based on the formation of built-in electric field identified by KPFM, the band diagram of graphene contacted with the GaN NPs was illustrated in Fig. 6c. The thin graphene film possessed high transparency at the UV range, and thus the irradiated UV light would penetrate from the graphene to GaN NPs. As the GaN NPs absorbing the photon energy of irradiated light larger than its bandgap, electron-hole pairs would be generated. With the assistance of the built-in electric field at the interface of the graphene and GaN NPs, the photo-generated electrons would drift into graphene and remain opposite holes in the GaN NPs. In the front part, we have demonstrated the graphene is in p-type dopant. Therefore, the recombination between the intrinsic holes and photo-generated electrons drifted in graphene could result in attenuation of holes conduction, which further decreased the measured current through graphene driven by the bias voltage, which was the origin of the negative photocurrent phenomenon in the GaN NPs/graphene UV PDs. Besides, the electron drifted into graphene resulted in the E_F of graphene up-shifting to the Dirac point, further lowering the built-in electric field at the interface of graphene and GaN NPs [50]. Therefore, the stronger incident laser powers induced photo-generated carriers would gradually weaken the built-in electric field as well as the drifted efficiency of photo-generated electron into graphene, illustrating the decreased responsivity as the function incident powers.

The corresponding carrier transport model of the GaN NPs/graphene UV PDs was established in Fig. 6d. The trap states have made holes in the GaN NPs a longer carrier lifetime, and it was also suitable for opposite electron drifted into graphene. At the same time, the graphene possessed high carrier mobility, which made the photo-generated electron in graphene transporting very fast with the applied bias voltage, further inducing the persistent photoconduction effect in the GaN NPs/graphene UV PDs. The dynamic carrier transfer process in the UV PDs was confirmed by the UV light-assisted KPFM, as shown in Fig. S6. The KPFM scan region was divided into three states: original dark condition, UV light irradiation

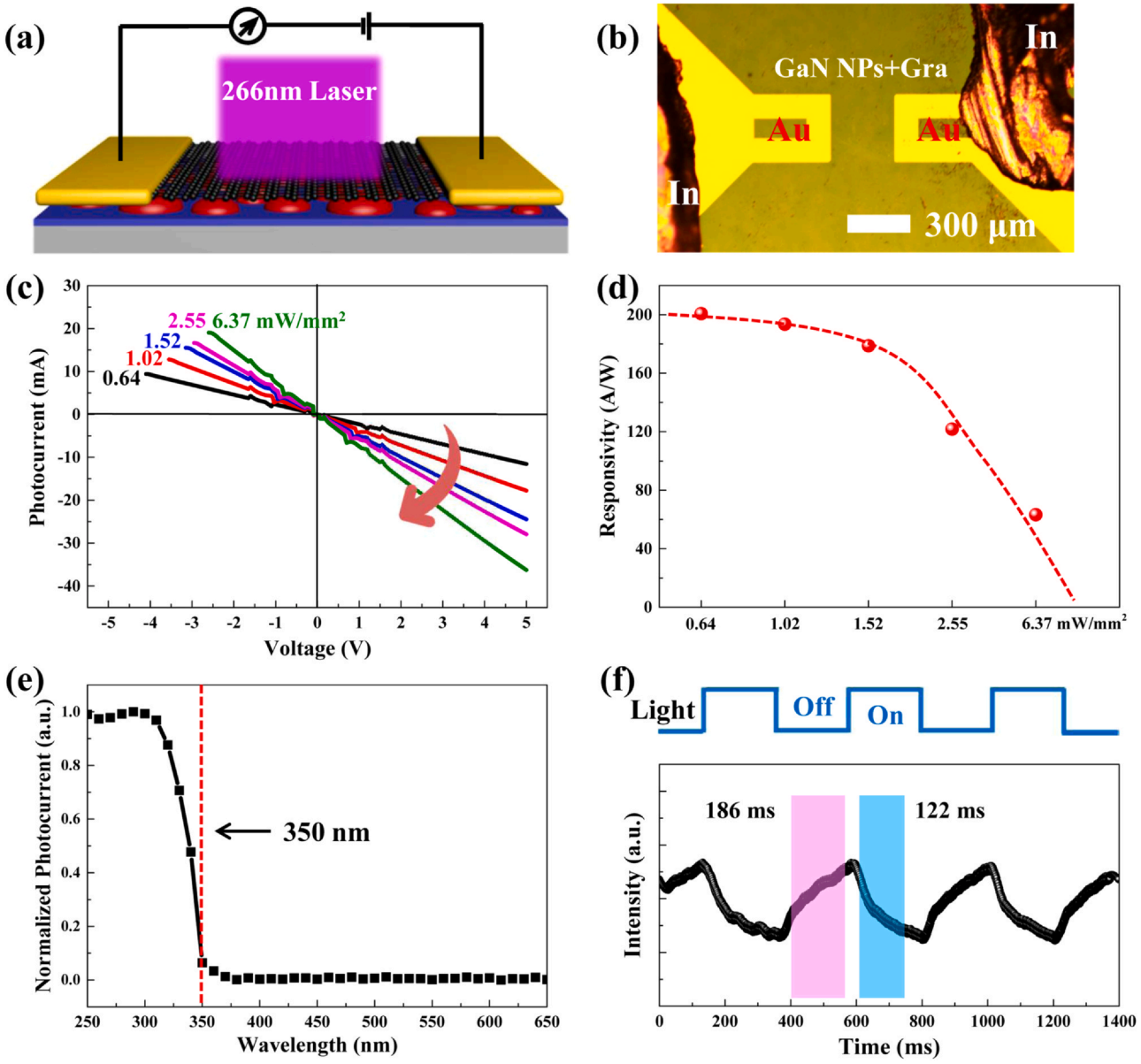

Fig. 5. (a) Schematic device structure and (b) optical image of the UV PDs based on the GaN NPs and graphene. (c) Photocurrent as a function of bias voltage under different incident power. (d) Responsivity as a function of incident power at bias voltage of 5 V. (e) Response spectra at the wavelength of 250–650 nm and (f) response time of the UV PDs.

Table 1
Comparison of the device performance for the GaN NPs/grephene-based UV PDs and the related devices in previous works.

GaN type	Graphene type	Bias voltage (V)	Dark current (A)	Responsivity (A/W)	Photosensitivity (%)	Quantum efficiency	Response time (ms)	Light source	Ref.
Ga_2O_3/GaN nanowire	CVD-grown	-5	5.42×10^{-8}	753.2	—	22.5	80/160	364 nm LED	[11]
InGaN dot	CVD-grown	1	—	1.6×10^{9}	—	—	200/10^5	450 nm	[18]
GaN epilayer	CVD-grown	-10	2.9×10^{-4}	5.83	—	22	2.7/4.6	325 nm Laser	[25]
GaN epilayer	CVD-grown	10	$> 1 \times 10^{-4}$	0.361	—	1.38	5.05/5.11	325 nm Laser	[26]
GaN epilayer	r-GO	0	6.2×10^{-9}	1.54×10^{-3}	85	—	60/267	350 nm Lamp	[50]
GaN nanowire	CVD-grown	1	4.3×10^{-5}	25	—	—	—	357 nm LED	[51]
AlGaN nanowire	CVD-grown	-2	5.4×10^{-8}	1.76×10^{-4}	—	—	4000/4700	347 nm	[52]
GaN epilayer	Growth from PMMA	10	—	4	—	—	7.2/18.2	266 nm Laser	[53]
GaN NP	CVD-grown	5	6.85×10^{-2}	200.69	52.9	0.94×10^{3}	122/186	266 nm Laser	**This work**

condition, and UV light removal condition. The surface potential of graphene on the GaN NPs increased after the UV light irradiation, implying the up-shift of E_F for graphene as well as the reduction of hole density by recombination with the drifted electrons. This was consistent with the fact that photo-generated electron of the GaN NPs drifted into graphene under the built-in electric field. Moreover, the remained high surface potential of graphene after the UV light removal condition has demonstrated the persistent photoconduction effect in graphene. As a result, the fast circulation of carriers in graphene driven by the bias voltage would induce the high

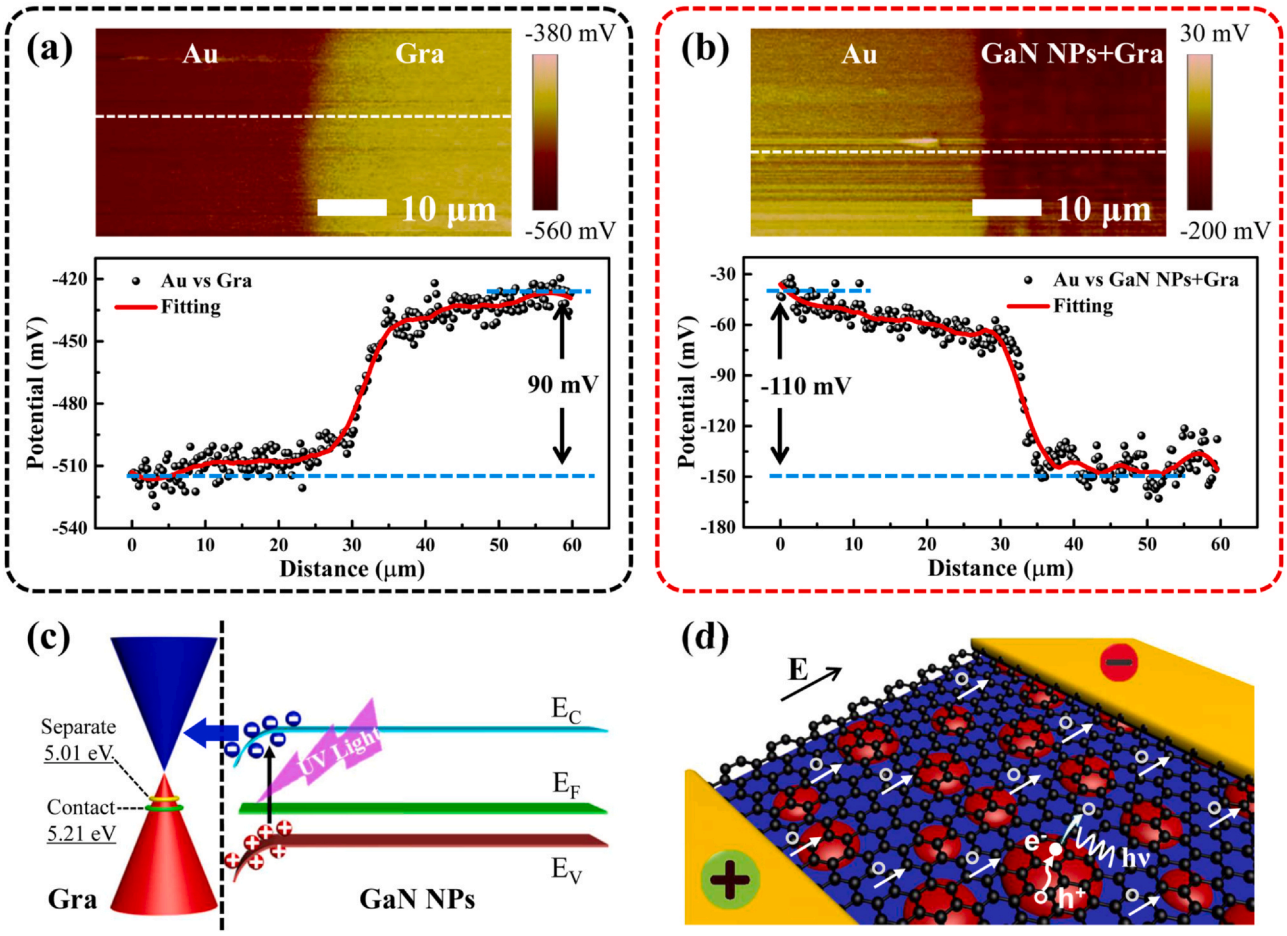

Fig. 6. (a) Surface potential of separated graphene and (b) graphene contacted with the GaN NPs. (c) Band diagram and carrier transfer between the GaN NPs and graphene with the irradiation of UV light. (d) The schematic diagram of the carrier transport model for the UV PDs with GaN NPs and graphene.

responsivity. It should be noted that the persistent photoconduction effect in the GaN NPs/graphene UV PDs also resulted in the increased response time, which might be solved by adding gate electrodes to adjust the built-in electric field at the interface of the GaN NPs and graphene.

4. Conclusions

In conclusion, we have grown the GaN NPs on the AlN template by the Ga droplets epitaxy method in HT-MOCVD system. The excellent properties of the GaN NPs were evaluated by the SEM, AFM, XPS, EDS, and temperature-dependent PL spectra. The high-response UV PDs were demonstrated by integrating the GaN NPs absorber with graphene carrier transport channel, and the high responsivity of 200.69 A/W has been achieved at the bias voltage of 5 V. This value was almost two orders of magnitude higher than that of based on the generally used GaN epilayer. The carrier transport model and work mechanism of the device were verified by the KPFM measurement, proving that the trap states in GaN NPs induced the longer lifetime of the photo-generated carriers as well as the persistent photoconduction effect in the graphene layer. The present work could be extended into the PDs with detected wavelength covered from deep UV to visible ranges by incorporating Al and In atoms in present GaN NPs, such as AlGaN and InGaN NPs, which were supposed to be the next generation III-nitrides-based PDs with high sensitivity.

CRediT authorship contribution statement

The manuscript was written through contributions of all authors. All authors have given approval to the final version of the manuscript.

Declaration of Competing Interest

The authors declare that they have no known competing financial interests or personal relationships that could have appeared to influence the work reported in this paper.

Acknowledgements

This work was supported by the National Natural Science Foundation of China (61922078, 61874118, 61725403, 61704171, 52002368), China; National Key Research and Development Program of China (2017YFB0404103), China; Youth Innovation Promotion Association of the Chinese Academy of Sciences (Y201945), China; The Open Project of State Key Laboratory of Luminescence and Applications (E00522NZM100), China; Key-Area Research and Development Program of Guangdong Province (2020B010169001), China; Suzhou Institute of Nano-Tech and Nano-Bionics (20YZ10), China.

Appendix A. Supporting information

Supplementary data associated with this article can be found in the online version at doi:10.1016/j.jallcom.2021.159281.

References

[1] D.B. Li, K. Jiang, X.J. Sun, C.L. Guo, AlGaN photonics: recent advances in materials and ultraviolet devices, Adv. Opt. Photonics 10 (2018) 43–110.
[2] W.Y. Zou, M. Sastry, J.J. Gooding, R. Ramanathan, V. Bansal, Recent advances and a roadmap to wearable UV sensor technologies, Adv. Mater. Technol. 5 (2020) 1901036.
[3] R. Rehm, R. Driad, L. Kirste, S. Leone, T. Passow, F. Rutz, L. Watschke, A. Zibold, Toward AlGaN focal plane arrays for solar-blind ultraviolet detection, Phys. Status Solidi A 217 (2020) 1900769.
[4] Q. Liu, Y.Q. Yang, X.F. Wang, W.D. Song, X.J. Luo, J.Q. Guo, J. Shi, C. Cheng, D.Y. Li, L.F. He, K. Li, F.L. Gao, S.T. Li, High-performance UV–visible photodetectors based on CH3NH3PbI3-Cl /GaN microwire array heterostructures, J. Alloy. Compd. 864 (2021) 158710.
[5] A. Dubey, R. Mishra, Y.H. Hsieh, C.W. Cheng, B.H. Wu, L.J. Chen, S. Gwo, T.J. Yen, Aluminum plasmonics enriched ultraviolet gan photodetector with ultrahigh responsivity, detectivity, and broad bandwidth, Adv. Sci. 7 (2020) 2002274.
[6] N. Prakash, G. Kumar, M. Singh, S.P. Singh, B. Satpati, S.P. Khanna, P. Pal, Long-Term, high-voltage, and high-temperature stable dual-mode, low dark current broadband ultraviolet photodetector based on solution-cast r-GO on MBE-grown highly resistive GaN, Adv. Opt. Mater. 7 (2019) 1900340.
[7] N. Aggarwal, S. Krishna, S.K. Jain, A. Arora, L. Goswami, A. Sharma, S. Husale, A. Gundimeda, G. Gupta, Impact on photon-assisted charge carrier transport by engineering electrodes of GaN based UV photodetectors, J. Alloy. Compd. 785 (2019) 883–890.
[8] J.D. Yu, L. Wang, Z.B. Hao, Y. Luo, C.Z. Sun, J. Wang, Y.J. Han, B. Xiong, H.T. Li, Van der Waals epitaxy of III-nitride semiconductors based on 2D materials for flexible applications, Adv. Mater. 32 (2020) 1903407.
[9] O. Saket, J. Wang, N. Amador-Mendez, M. Morassi, A. Kunti, F. Bayle, S. Collin, A. Jollivet, A. Babichev, T. Sodhi, J.C. Harmand, F.H. Julien, N. Gogneau, M. Tchernycheva, Investigation of the effect of the doping order in GaN nanowire p–n junctions grown by molecular-beam epitaxy, Nanotechnology 32 (2021) 085705.
[10] M. Spies, J. Polaczyński, A. Ajay, D. Kalita, M.A. Luong, J. Lähnemann, B. Gayral, M.I. den Hertog, E. Monroy, Effect of the nanowire diameter on the linearity of the response of GaN-based heterostructured nanowire photodetectors, Nanotechnology 29 (2018) 255204.
[11] T. He, X.D. Zhang, X.Y. Ding, C. Sun, Y.K. Zhao, Q. Yu, J.Q. Ning, R.X. Wang, G.H. Yu, S.L. Lu, K. Zhang, X.P. Zhang, B.S. Zhang, Broadband ultraviolet photodetector based on vertical Ga_2O_3/GaN nanowire array with high responsivity, Adv. Opt. Mater. 7 (2019) 1801563.
[12] A. Aiello, A.K.M.H. Hoque, M.Z. Baten, P. Bhattacharya, High-gain silicon-based InGaN/GaN dot-in-nanowire array photodetector, ACS Photonics 6 (2019) 1289–1294.
[13] L. Wang, L. Wang, J.D. Yu, Z.B. Hao, Y. Luo, C.Z. Sun, Y.J. Han, B. Xiong, J. Wang, H.T. Li, Abnormal stranski–krastanov mode growth of green ingan quantum dots: morphology, optical properties, and applications in light-emitting devices, ACS Appl. Mater. Interfaces 11 (2019) 1228–1238.
[14] S. Tamariz, G. Callsen, N. Grandjean, Density control of GaN quantum dots on AlN single crystal, Appl. Phys. Lett. 114 (2019) 082101.
[15] Z.Q. Qi, S.L. Li, X.H. Huang, S.C. Sun, W. Zhang, W. Ye, J.N. Dai, Z.H. Wu, C.Q. Chen, Y. Tian, Y.Y. Fang, Influence of high-temperature postgrowth annealing under different ambience on GaN quantum dots grown via Ga droplet epitaxy, Opt. Mater. Express 5 (2015) 1598–1605.
[16] C.Y. Tsai, Y.Z. Su, I.S. Yu, Effects of temperature and nitradition on phase transformation of GaN quantum dots grown by droplet epitaxy, Surf. Coat. Tech. 358 (2019) 182–189.
[17] H. Lu, C. Reese, S. Jeon, A. Sundar, Y. Fan, E. Rizzi, Y. Zhuo, L. Qi, R.S. Goldman, Mechanisms of GaN quantum dot formation during nitridation of Ga droplets, Appl. Phys. Lett. 116 (2020) 062107.
[18] A.Q. Hu, H.J. Tian, Q.L. Liu, L. Wang, L. Wang, X.Y. He, Y. Luo, X. Guo, Graphene on self-assembled InGaN quantum dots enabling ultrahighly sensitive photodetectors, Adv. Opt. Mater. 7 (2019) 1801792.
[19] C. Hu, X.J. Wang, B. Song, High-performance position-sensitive detector based on the lateral photoelectrical effect of two-dimensional materials, Light Sci. Appl. 9 (2020) 88.
[20] J.Y. Han, M.Y. He, M. Yang, Q. Han, F. Wang, F. Zhong, M.J. Xu, Q. Li, H. Zhu, C.X. Shan, W.D. Hu, X.Q. Chen, X.R. Wang, J. Gou, Z.M. Wu, J. Wang, Light-modulated vertical heterojunction phototransistors with distinct logical photocurrents, Light Sci. Appl. 9 (2020) 167.
[21] J. Thakur, H.S. Saini, M. Singh, A.H. Reshak, M.K. Kashyap, Quest for magnetism in graphene via Cr- and Mo-doping: a DFT approach, Phys. E 78 (2016) 35–40.
[22] J. Thakur, M.K. Kashyap, H.S. Saini, A.H. Reshak, Half metallicity and magnetism in graphene containing monovacancies decorated with carbon/nitrogen adatom, J. Alloy. Compd. 663 (2016) 100–106.
[23] J. Thakur, M.K. Kashyap, A. Taya, P. Rani, H.S. Saini, A.H. Reshak, Structure stability and magnetism in graphene impurity complexes with embedded V and Nb atoms, J. Magn. Magn. Mater. 433 (2017) 109–115.
[24] A.H. Reshak, Chairlike and boatlike graphane: active photocatalytic water splitting solar-to-hydrogen energy conversion under UV irradiation, J. Phys. Chem. C. 122 (2018) 8076–8081.
[25] H.J. Tian, Q.L. Liu, C.X. Zhou, X.J. Zhan, X.Y. He, A.Q. Hu, X. Guo, Hybrid graphene/unintentionally doped GaN ultraviolet photodetector with high responsivity and speed, Appl. Phys. Lett. 113 (2018) 121109.
[26] H.J. Tian, Q.L. Liu, A.Q. Hu, X.Y. He, Z.H. Hu, X. Guo, Hybrid graphene/GaN ultraviolet photo-transistors with high responsivity and speed, Opt. Express 26 (2018) 5408–5415.
[27] B. Pandit, E.F. Schubert, J. Cho, Dual-functional ultraviolet photodetector with graphene electrodes on AlGaN/GaN heterostructure, Sci. Rep. 10 (2020) 22059.
[28] X. Shen, D. Wang, J. Ning, B. Wang, H. Guo, C. Zhang, Y. Jia, J. Dong, X. Feng, X. Wang, J. Zhang, Y. Hao, MMA-enabled ultraclean graphene transfer for fast-response graphene/GaN ultraviolet photodetectors, Carbon 169 (2020) 92–98.
[29] J. Li, X. Xi, S. Lin, Z. Ma, X. Li, L. Zhao, Ultrahigh sensitivity graphene/nanoporous GaN ultraviolet photodetectors, ACS Appl. Mater. Interfaces 12 (2020) 11965–11971.
[30] Y. Wu, X.J. Sun, Z.M. Shi, Y.P. Jia, K. Jiang, J.W. Ben, C.H. Kai, Y. Wang, W. Lü, D.B. Li, In situ fabrication of Al surface plasmon nanoparticles by metal-organic chemical vapor deposition for enhanced performance of AlGaN deep ultraviolet detectors, Nanoscale Adv. 2 (2020) 1854–1858.
[31] Y. Chen, N. Zhang, Y.F. Li, Y.G. Bi, Y.Y. Yue, J. Feng, H.B. Sun, Microscale-patterned graphene electrodes for organic light-emitting devices by a simple patterning strategy, Adv. Opt. Mater. 6 (2018) 1701348.
[32] T. Kondo, K. Saitoh, Y. Yamamoto, T. Maruyama, S. Naritsuka, Fabrication of GaN dot structures on Si substrates by droplet epitaxy, Phys. Status Solidi A 203 (2006) 1700–1703.
[33] T. Maruyamaa, H. Otsuboa, T. Kondoa, Y. Yamamotob, S. Naritsuka, Fabrication of GaN dot structure by droplet epitaxy using NH_3, J. Cryst. Growth 301 (2007) 486–489.
[34] Z.Y. Chen, J.P. Zhao, T. Yano, T. Ooie, Valence band electronic structure of carbon nitride from x-ray photoelectron spectroscopy, J. Appl. Phys. 92 (2002) 281–287.
[35] J.B. Yang, T.C. Chang, J.J. Huang, S.C. Chen, P.C. Yang, Y.T. Chen, H.C. Tseng, S.M. Sze, A.K. Chu, M.J. Tsai, Resistive switching characteristics of gallium oxide for nonvolatile memory application, Thin Solid Films 529 (2013) 200–204.
[36] R. Huang, T. Liu, Y.F. Zhao, Y.F. Zhu, Z.L. Huang, F.S. Li, J.P. Liu, L.Q. Zhang, S.M. Zhang, A. Dingsun, H. Yang, Angular dependent XPS study of surface band bending on Ga-polar n-GaN, Appl. Surf. Sci. 440 (2018) 637–642.
[37] T.L. Duan, J.S. Pan, D.S. Ang, Interfacial chemistry and valence band offset between GaN and Al2O3 studied by X-ray photoelectron spectroscopy, Appl. Phys. Lett. 102 (2013) 201604.
[38] S.C. Wang, X. Zhang, Z.C. Feng, Y.P. Cui, Surface chemical and local electronic properties of AlxGa1-xN epi-layers grown by MOCVD, Opt. Express 22 (2014) 17440–17447.
[39] S. Sergent, S. Kako, M. Bürger, T. Schupp, D.J. As, Y. Arakawa, Excitonic complexes in single zinc-blende GaN/AlN quantum dots grown by droplet epitaxy, Appl. Phys. Lett. 105 (2014) 141112.
[40] P. Ramvall, P. Riblet, S. Nomura, Y. Aoyagi, S. Tanaka, Optical properties of GaN quantum dots, J. Appl. Phys. 87 (2000) 3883–3890.
[41] H.H. Yao, Y.T. Wang, M.C. Ou-yang, H.C. Kuo, S.C. Wang, C.F. Lin, Formation and optical properties of GaN/AlN multi-stacks with GaN nano-structures by metalorganic chemical vapour deposition, Nanotechnology 17 (2006) 664–667.
[42] Y. Chen, Y.Y. Yue, S.R. Wang, N. Zhang, J. Feng, H.B. Sun, Thermally-induced wrinkles on PH1000/graphene composite electrode for enhanced efficiency of organic solar cells, Sol. Energy Mater. Sol. Cells 201 (2019) 110075.
[43] A.C. Ferrari, J.C. Meyer, V. Scardaci, C. Casiraghi, M. Lazzeri, F. Mauri, S. Piscanec, D. Jiang, K.S. Novoselov, S. Roth, A.K. Geim, Raman spectrum of graphene and graphene layers, Phys. Rev. Lett. 97 (2006) 187401.
[44] Y.F. Hao, Y.Y. Wang, L. Wang, Z.H. Ni, Z.Q. Wang, R. Wang, C.K. Koo, Z.X. Shen, J.T.L. Thong, Probing layer number and stacking order of few-layer graphene by Raman spectroscopy, Small 6 (2010) 195–200.
[45] M.A. Mahdi, J.J. Hassan, S.S. Ng, Z. Hassan, N.M. Ahmed, Synthesis and characterization of single-crystal CdS nanosheet for high-speed photodetection, Phys. E 44 (2012) 1716–1721.
[46] Z.A. Bashkany, I.K. Abbas, M.A. Mahdi, H.F. Al-Taay, P. Jennings, A self-powered heterojunction photodetector based on a PbS nanostructure grown on porous silicon substrate, Silicon 10 (2018) 403–411.
[47] M.A. Mahdi, J.J. Hassan, N.M. Ahmed, S.S. Ng, Z. Hassan, Growth and characterization of CdS single-crystalline micro-rod photodetector, Superlattices Microstruct. 54 (2013) 137–145.
[48] A.A. Abdul-Hameed, M.A. Mahdi, B. Ali, A.M. Selman, H.F. Al-Taay, P. Jennings, W.-J. Lee, Fabrication of a high sensitivity and fast response self-powered photosensor based on a core-shell silicon nanowire homojunction, Superlattices Microstruct. 116 (2018) 27–35.
[49] J.S. Liu, C.X. Shan, B.H. Li, Z.Z. Zhang, C.L. Yang, D.Z. Shen, X.W. Fan, High responsivity ultraviolet photodetector realized via a carrier-trapping process, Appl. Phys. Lett. 97 (2010) 251102.
[50] N. Prakash, M. Singh, G. Kumar, A. Barvat, K. Anand, P. Pal, S.P. Singh, S.P. Khanna, Ultrasensitive self-powered large area planar GaN UV-photodetector using reduced graphene oxide electrodes, Appl. Phys. Lett. 109 (2016) 242102.

[51] A.V. Babichev, H. Zhang, P. Lavenus, F.H. Julien, A. Yu Egorov, Y.T. Lin, L.W. Tu, M. Tchernycheva, GaN nanowire ultraviolet photodetector with a graphene transparent contact, Appl. Phys. Lett. 103 (2013) 201103.
[52] M. Zhou, H.B. Qiu, T. He, J.Y. Zhang, W.X. Yang, S.L. Lu, L.F. Bian, Y.K. Zhao, UV Photodetector Based on Vertical (Al, Ga)N nanowires with graphene electrode and Si substrate, Phys. Status Solidi A 217 (2020) 2000061.
[53] Y. Chen, K. Jiang, H. Zang, J. Ben, S. Zhang, Z. Shi, Y. Jia, W. Lü, D. Li, X. Sun, Growth of high-quality wafer-scale graphene on dielectric substrate for high-response ultraviolet photodetector, Carbon 175 (2021) 155–163.
[54] J. Kierdaszuka, M. Tokarczyk, K.M. Czajkowski, R. Bożek, A. Krajewska, A. Przewłoka, W. Kaszub, M. Sobanska, Z.R. Zytkiewicz, G. Kowalski, T.J. Antosiewicz, M. Kamińska, A. Wysmołek, A. Drabińska, Surface-enhanced Raman scattering in graphene deposited on $Al_xGa_{1-x}N$/GaN axial heterostructure nanowires, Appl. Surf. Sci. 475 (2019) 559–564.
[55] Y.P. Jia, X.J. Sun, Z.M. Shi, K. Jiang, H.N. Liu, J.W. Ben, D.B. Li, Modulating the surface state of SiC to control carrier transport in graphene/SiC, Small 14 (2018) 1801273.
[56] D.B. Li, X.J. Sun, Y.P. Jia, M.I. Stockman, H.P. Paudel, H. Song, H. Jiang, Z.M. Li, Direct observation of localized surface plasmon field enhancement by Kelvin probe force microscopy, Light Sci. Appl. 6 (2017) e17038.